ChemComm

COMMUNICATION

View Article Online
View Journal | View Issue

Cite this: *Chem. Commun.*, 2024, **60**, 14045

Received 11th September 2024,
Accepted 1st November 2024

DOI: 10.1039/d4cc04679j

rsc.li/chemcomm

What could be the low-temperature limit of atomic layer deposition of platinum using $MeCpPtMe_3$ and oxygen?†

Hao Van Bui, *[a] Anh Phan Nguyen,[a] Manh Duc Dang,[a] Truong Duc Dinh,[a] Patricia J. Kooyman [b] and J. Ruud Van Ommen [c]

We explore the low-temperature limit of atomic layer deposition of Pt using $MeCpPtMe_3$ and O_2. We reveal that by supplying a sufficiently high O_2 exposure, highly dispersed and thermally stable Pt sub-nanometer clusters can be deposited onto the surface of P25 TiO_2 nanoparticles even at room temperature by atmospheric-pressure ALD.

Platinum nanoparticles (Pt NPs) supported on titanium dioxide (TiO_2) nanostructures have garnered significant attention in catalysis due to their exceptional catalytic activity, stability, and selectivity.[1,2] The combination of the excellent catalytic properties of Pt with the high surface area and strong metal–support interactions makes Pt/TiO_2 highly effective in both thermal and photocatalytic applications.[3–5] In addition, the synergy between Pt and TiO_2 enhances catalytic performance, particularly in photocatalysis, where Pt NPs act as electron sinks, reducing recombination rates of photogenerated electron–hole pairs, and thereby increasing the reaction efficiency.[6,7] Therefore, Pt/TiO_2 catalysts are widely used for pollutant degradation,[8,9] and various reactions such as hydrogen production from water splitting,[10,11] hydrogenation,[3,12] and oxidation reactions.[13,14]

The catalytic efficiency of Pt NPs is strongly correlated with their size.[13–17] Smaller Pt NPs offer a higher surface-to-volume ratio, increasing the availability of active sites for catalytic reactions. However, excessively small NPs can show decreased stability due to sintering and agglomeration.[18] Therefore, precise control over Pt nanoparticle size is crucial for optimizing catalytic performance, balancing high efficiency with long-term stability, and enabling tailored catalytic properties for specific reactions. With the capability of controlling the deposition at the atomic level,[19,20] atomic layer deposition (ALD) is a precise and controllable technique used to deposit Pt NPs onto different surfaces.[21–24] ALD employs sequential, self-limiting surface reactions to enable atomic-level control of the Pt particle size and dispersion, even on complex TiO_2 nanostructures, ensuring a high coverage of Pt NPs.[11,25,26] A typical Pt ALD process involves alternating exposures of the substrate to a Pt precursor vapor, such as $MeCpPtMe_3$, and an oxidizing agent, often oxygen (O_2) or ozone (O_3). This is the most widely employed Pt ALD process, which is commonly conducted at a temperature in the range of 200–300 °C.[27–29]

Our previous studies demonstrate that Pt NPs can be deposited on graphene nanoplatelets at 100 °C,[18,30] which is significantly lower than the deposition temperatures of other processes.[27–29] Such a low-temperature ALD process is enabled by a sufficiently high O_2 exposure (*i.e.*, >> 120 mbar·s) in the second half-reaction.[31] The low-temperature deposition significantly reduces the diffusion and coalescence of the deposited Pt NPs, enabling size-controlled growth, which is highly essential for Pt NPs-based catalysts. The findings of the previous studies raise the question of what the low-temperature limit of this ALD process could be, which motivates our current study. Here, we further investigate the influence of temperature on the deposition of Pt NPs on TiO_2 surface in ALD using $MeCpPtMe_3$ and O_2. We demonstrate that lowering the deposition temperature results in a better control of the particle size, and even enables the deposition of highly dispersed Pt sub-nanometer clusters at room temperature. The subsequent calcination at a relatively high temperature reveals high stability and strong metal–support interactions of the room-temperature deposited Pt nanoclusters.

Pt was deposited on a gram-scale quantity of TiO_2 nanopowder (Evonik P25 TiO_2) using a fluidized bed reactor operating at atmospheric pressure, as detailed in the ESI.† TEM images of Pt NPs deposited on the surface of P25 TiO_2 at 250 °C after 5 ALD cycles are presented in Fig. 1a and Fig. S1 (ESI†). The corresponding particle size distribution (PSD) is shown in Fig. 1b. The results indicate that the Pt NPs deposited at 250 °C are

[a] *Faculty of Materials Science and Engineering, Phenikaa University, Yen Nghia, Ha Dong District, Hanoi 12116, Vietnam. E-mail: hao.buivan@phenikaa-uni.edu.vn*
[b] *Catalysis Institute, Department of Chemical Engineering, University of Cape Town, Private Bag X3, Rondebosch 7701, South Africa*
[c] *Department of Chemical Engineering, Delft University of Technology, Van der Maasweg 9, Delft, 2629 HZ, The Netherlands*

† Electronic supplementary information (ESI) available. See DOI: https://doi.org/10.1039/d4cc04679j

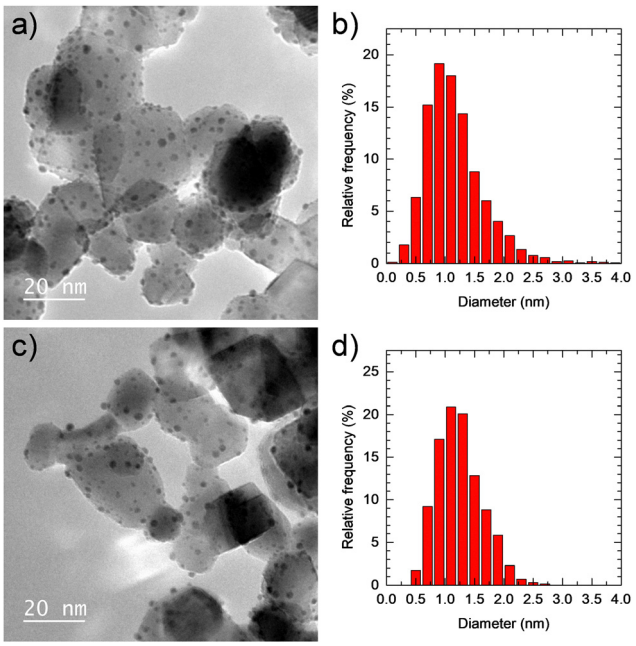

Fig. 1 TEM images and PSDs of Pt NPs deposited on P25 TiO_2 surface at 250 °C (a) and (b) and 150 °C (c) and (d) after 5 ALD cycles.

highly dispersed on the surface. The mean diameter of the Pt NPs is found to be 1.2 nm with a standard deviation of 0.5 nm. However, the particle size spans from 0.2 to 4 nm, resulting in a broad right-skewed PSD although the number of NPs larger than 3 nm accounts for only less than 1% of the total number of NPs analysed. This resembles the PSD of Pt NPs deposited on graphene nanoplatelets at high temperatures.[18,30] Such a broad and right-skewed PSD is the result of the diffusion and coalescence of Pt NPs due to their high mobility at high temperatures, in addition to their on-going growth.[18] The broad PSD is also caused by the continuous formation of new nuclei, which generally occurs during the deposition of nanoparticles, even in wet-chemistry methods.[32] This accounts for the nucleation peak on the left side of the PSD. Both the coalescence and the new nuclei formation can be reduced by lowering the deposition temperature, which is evidenced by the TEM images and PSD of the Pt NPs deposited at 150 °C shown in Fig. 1c and d and Fig. S2 (ESI†). In this case, the average particle size and the standard deviation are found to be 1.3 nm and 0.4 nm, respectively. The particle size spans from 0.4 to 2.6 nm, resulting in a narrower PSD. Importantly, the comparison of the two PSDs reveals that the center of the PSD of Pt NPs deposited at 150 °C shifts to the right side (Fig. S3, ESI†). This is an indication of the preferential deposition of Pt on the previously formed Pt NPs rather than the formation of new nuclei.

Further lowering the deposition temperature significantly alters the growth mechanism of Pt NPs. This is indicated by the TEM images and PSDs of Pt NPs deposited at 100 °C after 1, 5 and 10 ALD cycles shown in Fig. 2 and Fig. S4 (ESI†). The TEM images qualitatively indicate that both the size of Pt NPs and their spatial distribution on P25 TiO_2 surface are highly uniform, which is reflected by the significantly narrower PSDs. The

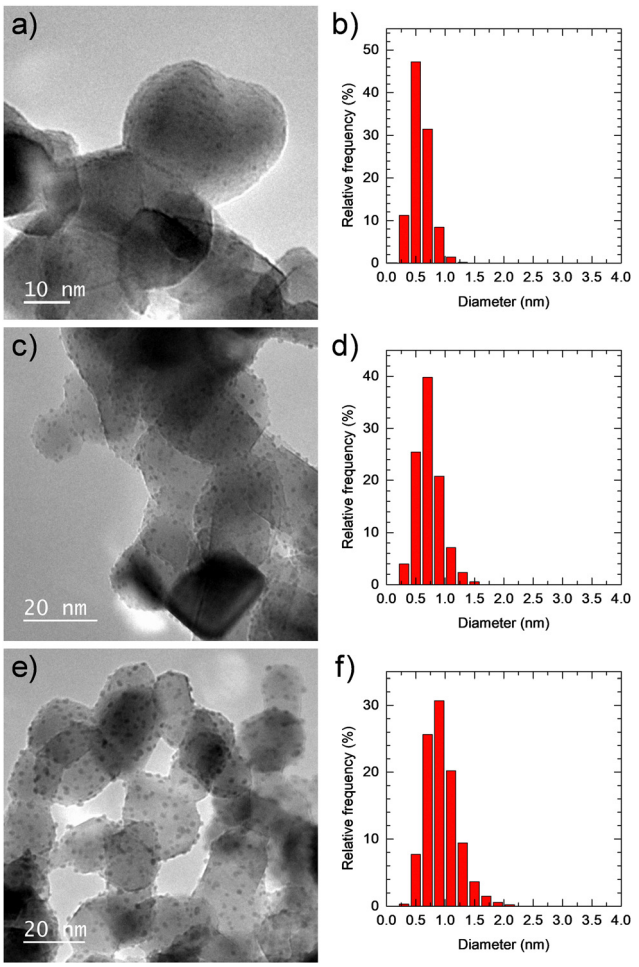

Fig. 2 TEM images and PSDs of Pt NPs deposited on P25 TiO_2 surface at 100 °C after 1 cycle (a) and (b), 5 cycles (c) and (d) and 10 cycles (e) and (f).

comparison of the PSD in Fig. 2d with those in Fig. 1b and d (see also Fig. S3, ESI†) reveals that the PSD of Pt NPs deposited at 100 °C shifts substantially to the left side. This contrasts with the shift of the PSD of Pt NPs deposited at 150 °C, which can be explained by the effective hindrance of both the coalescence of Pt NPs and the formation of new nuclei at 100 °C. Instead, the deposition takes place mainly on the surface of previously formed Pt NPs. This enables the capability of controlling the particle size by the number of ALD cycles, as demonstrated in Fig. 2. With increasing the number of ALD cycles, the entire PSD shifts gradually to the right side (Fig. S5, ESI†) while retaining its narrowness. The results indicate that lowering the temperature offers great advantages in controlling the Pt NPs size, which is a crucial factor in catalysis.

Other studies have demonstrated that thermal ALD of Pt using $MeCpPtMe_3$ and O_2 could only be conducted typically in the temperature range of 200–300 °C,[27–29] and no studies have been successful in depositing Pt NPs using this process at a temperature below 150 °C, unless using O_3 as the reactant.[33] Our previous work has revealed that the unsuccessful depositions arise from insufficient O_2 exposure in the second half-cycle.[31] We have proved that, even at 300 °C, for the same Pt precursor

dosage, insufficient O_2 exposure hampers Pt deposition,[31] whereas at 100 °C sufficiently high O_2 exposure enables the deposition of highly uniform and excellent size-controlled Pt NPs.[18,30] Our present study further confirms the pivotal role of O_2 exposure, and in all studies, the lower deposition temperature provides the better control of Pt NP growth. This cannot be achieved for the deposition at high temperatures, as observed for ALD of Pt on graphene and P25 TiO_2.[18,30,34,35]

To further explore the low-temperature limit of the $MeCpPtMe_3/O_2$ ALD chemistry, we conducted experiments at room temperature. When the same O_2 exposure as for ALD at 100–250 °C is applied (*i.e.*, 5 min at a partial pressure of 200 mbar), there is virtually no trace of Pt NPs on the P25 TiO_2 surface after 5 ALD cycles. However, upon an increase in the O_2 exposure of 6 times (*i.e.*, the "pulse" time increases from 5 min to 30 min), highly dispersed Pt sub-nanometer clusters (Pt s-NCs) are observed, as shown in Fig. 3a and Fig. S6 (ESI†). The HAADF-TEM images indicate a high density of Pt s-NCs on the surface with an average cluster size of 0.6 nm and a standard deviation of 0.2 nm. The PSD in Fig. 3b shows a remarkably narrow distribution, in which the cluster size spans from 0.2 to 1.3 nm with only less than 2.8% of the clusters being larger than 1 nm. The formation of a high density of Pt s-NCs indicates that the surface reactions between the Pt precursor molecules and O_2 already take place at room temperature.[31] Nevertheless, this only occurs for considerably long O_2 exposure, indicating slow kinetics of the reactions. Importantly, the X-ray photoelectron spectroscopic analysis (Fig. S7, ESI†) indicates the metallic state of Pt s-NCs, which is strong evidence of the successful deposition of Pt at room temperature.

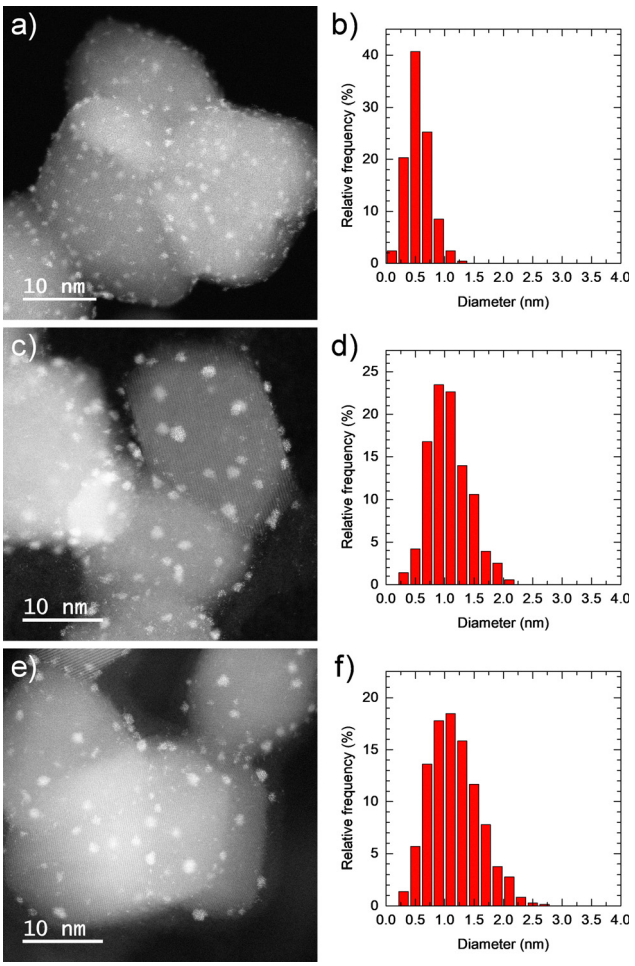

Fig. 3 HAADF-STEM images and PSDs of Pt s-NCs/NPs deposited on P25 TiO_2 surface at room temperature (*i.e.*, 25 °C) after 5 ALD cycles (a) and (b), followed by the annealing in air at 400 °C for 3 h (c) and (d) and 6 h (e) and (f).

The thermal stability of the Pt s-NCs is evaluated by annealing them in ambient air at 400 °C for 3 and 6 h. The TEM images and PSDs of the Pt s-NCs after annealing are shown in Fig. 3c–f, Fig. S6, and S8 (ESI†). The results indicate the coalescence of Pt s-NCs, forming Pt NPs. However, in comparison with those obtained by ALD at 250 and 150 °C, the coalescence caused by the annealing is much less severe despite being conducted at a higher temperature and for a longer processing time. This is because the coalescence of Pt NPs mainly takes place during the O_2 exposure step of ALD cycles (*i.e.*, in the second half-cycle), which is enhanced by the local heat generated by the combustion of the precursor ligands by O_2.[18] Importantly, a large number of Pt single atoms are found on the surface of TiO_2 after the annealing. This indicates that Pt single atoms are strongly bound to the surface, suggesting a strong metal–support interaction between the Pt single atoms and TiO_2, which is of great importance in heterogeneous catalysis.[36,37]

Overall, the PSDs of Pt NPs and s-NCs obtained after 5 ALD cycles under different ALD and post treatment conditions are summarized by the box-and-whisker plots shown in Fig. S9 (ESI†). The figure indicates that the PSDs of Pt deposited at room temperature (RT) and at 100 °C exhibit the narrowest spans and smallest average diameters. Additionally, the smaller vertical dimension of the boxes indicates the higher density of the Pt NPs/s-NCs near the average diameter. The results demonstrate great advantages of low-temperature deposition in enabling the deposition of highly dispersed and uniform Pt s-NCs and NPs, which have been demonstrated as highly efficient catalysts for various catalytic reactions.[37–39]

In conclusion, our work demonstrates that the low-temperature limit of the Pt ALD using $MeCpPtMe_3$ and O_2 can be extended to room temperature by supplying a sufficiently high O_2 exposure. The room-temperature process effectively hinders diffusion and coalescence, enabling the deposition of a high density of Pt sub-nanometer clusters onto the surface of P25 TiO_2 nanoparticles. The post-annealing in ambient air at 400 °C causes coalescence of Pt s-NCs, however, it is much less severe in comparison with the coalescence taking place during ALD at 150 and 250 °C. Our approach of low-temperature deposition may pave the way for the optimized synthesis of Pt-supported catalysts that can maximize the Pt usage efficiency and catalytic performance by controlling both the particle size and distribution over the support.

This work is funded by Phenikaa Innovation Foundation (Phenikaa Group), under the grant number ĐMST-2022.03. This work is additionally based on the research supported in part by the National Research Foundation of South Africa, Grant number 94878. The authors acknowledge Prof. Il-Kwon Oh and Aerim Choi at Ajou University, South Korea, for the XPS

analysis, and the Centre for High Resolution Transmission Electron Microscopy at Nelson Mandela Metropolitan University in Port Elizabeth for the use of the facilities.

Data availability

The data supporting this article have been included as part of the ESI.†

Conflicts of interest

There are no conflicts to declare.

References

1 M. Tasbihi, F. Fresno, U. Simon, I. J. Villar-García, V. Pérez-Dieste, C. Escudero and V. A. de la Peña O'Shea, *Appl. Catal., B*, 2018, **239**, 68–76.
2 X. Chen, X. Su, H. Duan, B. Liang, Y. Huang and T. Zhang, *Catal. Today*, 2017, **281**, 312–318.
3 L. R. Baker, G. Kennedy, M. Van Spronsen, A. Hervier, X. Cai, S. Chen, L.-W. Wang and G. A. Somorjai, *J. Am. Chem. Soc.*, 2012, **134**, 14208–14216.
4 B. Han, Y. Guo, Y. Huang, W. Xi, J. Xu, J. Luo, H. Qi, Y. Ren, X. Liu, B. Qiao and T. Zhang, *Angew. Chem., Int. Ed.*, 2020, **59**, 11824–11829.
5 J. Lu, J. W. Elam and P. C. Stair, *Acc. Chem. Res.*, 2013, **46**, 1806–1815.
6 A. Naldoni, M. D'Arienzo, M. Altomare, M. Marelli, R. Scotti, F. Morazzoni, E. Selli and V. Dal Santo, *Appl. Catal., B*, 2013, **130–131**, 239–248.
7 S. Kattel, B. Yan, J. G. Chen and P. Liu, *J. Catal.*, 2016, **343**, 115–126.
8 F. B. Li and X. Z. Li, *Chemosphere*, 2002, **48**, 1103–1111.
9 A. Goulas and J. R. van Ommen, *J. Mater. Chem. A*, 2013, **1**, 4647–4650.
10 K. Matsubara, M. Inoue, H. Hagiwara and T. Abe, *Appl. Catal., B*, 2019, **254**, 7–14.
11 Y. Chen, Y. Wang, L. Zheng, Y. Chang, S. Xu, Y. Wu, W. Zhou, Y. Lu, J. Wang and H. Li, *Mater. Today Energy*, 2022, **27**, 101042.
12 M. Macino, A. J. Barnes, S. M. Althahban, R. Qu, E. K. Gibson, D. J. Morgan, S. J. Freakley, N. Dimitratos, C. J. Kiely, X. Gao, A. M. Beale, D. Bethell, Q. He, M. Sankar and G. J. Hutchings, *Nat. Catal.*, 2019, **2**, 873–881.
13 N. Li, Q.-Y. Chen, L.-F. Luo, W.-X. Huang, M.-F. Luo, G.-S. Hu and J.-Q. Lu, *Appl. Catal., B*, 2013, **142–143**, 523–532.
14 G. J. Kim, D. W. Kwon and S. C. Hong, *J. Phys. Chem. C*, 2016, **120**, 17996–18004.
15 M. Arenz, K. J. J. Mayrhofer, V. Stamenkovic, B. B. Blizanac, T. Tomoyuki, P. N. Ross and N. M. Markovic, *J. Am. Chem. Soc.*, 2005, **127**, 6819–6829.
16 W. Zhang, H. Wang, J. Jiang, Z. Sui, Y. Zhu, D. Chen and X. Zhou, *ACS Catal.*, 2020, **10**, 12932–12942.
17 J. Zhu, M.-L. Yang, Y. Yu, Y.-A. Zhu, Z.-J. Sui, X.-G. Zhou, A. Holmen and D. Chen, *ACS Catal.*, 2015, **5**, 6310–6319.
18 F. Grillo, H. Van Bui, J. A. Moulijn, M. T. Kreutzer and J. R. van Ommen, *J. Phys. Chem. Lett.*, 2017, **8**, 975–983.
19 H. Van Bui, F. Grillo and J. R. Van Ommen, *Chem. Commun.*, 2017, **53**, 45–71.
20 J. Fonseca and J. Lu, *ACS Catal.*, 2021, **11**, 7018–7059.
21 J. Li, X. Liang, D. M. King, Y.-B. Jiang and A. W. Weimer, *Appl. Catal., B*, 2010, **97**, 220–226.
22 W.-J. Lee, Z. Wan, C.-M. Kim, I.-K. Oh, R. Harada, K. Suzuki, E.-A. Choi and S.-H. Kwon, *Chem. Mater.*, 2019, **31**, 5056–5064.
23 W.-J. Lee, S. Bera, H.-C. Shin, W.-P. Hong, S.-J. Oh, Z. Wan and S.-H. Kwon, *Adv. Mater. Interfaces*, 2019, **6**, 1901210.
24 K.-H. T. Dinh, H. T. T. Ta, N. L. Nguyen, V. T. Le, V. H. Nguyen and H. Van Bui, *Chem. Mater.*, 2023, **35**, 2248–2280.
25 J. Zhang, Z. Yu, Z. Gao, H. Ge, S. Zhao, C. Chen, S. Chen, X. Tong, M. Wang, Z. Zheng and Y. Qin, *Angew. Chem., Int. Ed.*, 2017, **56**, 816–820.
26 J. Zhang, W. Yu, D. Feng, H. Xu and Y. Qin, *Appl. Catal., B*, 2022, **312**, 121405.
27 Y. Zhou, D. M. King, X. Liang, J. Li and A. W. Weimer, *Appl. Catal., B*, 2010, **101**, 54–60.
28 T. Aaltonen, M. Ritala, Y.-L. Tung, Y. Chi, K. Arstila, K. Meinander and M. Leskelä, *J. Mater. Res.*, 2004, **19**, 3353–3358.
29 H.-B.-R. Lee and S. F. Bent, *Chem. Mater.*, 2012, **24**, 279–286.
30 H. Van Bui, F. Grillo, S. Sharath Kulkarni, R. Bevaart, N. V. Thang, B. van der Linden, J. A. Moulijn, M. Makkee, M. T. Kreutzer and J. R. van Ommen, *Nanoscale*, 2017, **9**, 10802–10810.
31 F. Grillo, H. Van Bui, D. La Zara, A. A. I. Aarnink, A. Y. Kovalgin, P. Kooyman, M. T. Kreutzer and J. R. van Ommen, *Small*, 2018, **14**, 1800765.
32 M. A. Watzky and R. G. Finke, *J. Am. Chem. Soc.*, 1997, **119**, 10382–10400.
33 J. Dendooven, R. K. Ramachandran, K. Devloo-Casier, G. Rampelberg, M. Filez, H. Poelman, G. B. Marin, E. Fonda and C. Detavernier, *J. Phys. Chem. C*, 2013, **117**, 20557–20561.
34 J. R. van Ommen and A. Goulas, *Mater. Today Chem.*, 2019, **14**, 100183.
35 S. Sun, G. Zhang, N. Gauquelin, N. Chen, J. Zhou, S. Yang, W. Chen, X. Meng, D. Geng, M. N. Banis, R. Li, S. Ye, S. Knights, G. A. Botton, T.-K. Sham and X. Sun, *Sci. Rep.*, 2013, **3**, 1775.
36 H. Tang, F. Dong, S. Chen, J. Huang, F. Hong, Y. Su, G. Bai and B. Qiao, *ACS Catal.*, 2024, DOI: **10.1021/acscatal.4c03421**.
37 Z. Luo, X. Han, Z. Ma, B. Zhang, X. Zheng, Y. Liu, M. Gao, G. Zhao, Y. Lin, H. Pan and W. Sun, *Angew. Chem., Int. Ed.*, 2024, **63**, e202406728.
38 M. Tian, Z. Huang, J. Ni, W. Chen, Q. Zhou, H. Shen, X. Wu, H. Zhao and G. Jing, *Appl. Surf. Sci.*, 2024, **655**, 159515.
39 H. V. Thang, G. Pacchioni, L. DeRita and P. Christopher, *J. Catal.*, 2018, **367**, 104–114.

